Measurable structure factors of dense dispersions containing polydisperse optically inhomogeneous particles

Joel Diaz Maier, Katharina Gaus and Joachim Wagner*

Institut für Chemie, Universität Rostock, 18051 Rostock, Germany. *Correspondence e-mail: joachim.wagner@uni-rostock.de

Here, it is investigated how optical properties of single scatterers in interacting multi-particle systems influence measurable structure factors. Both particles with linear gradients of their scattering length density and core–shell structures evoke characteristic deviations between the weighted sum $\langle S(Q) \rangle$ of partial structure factors in a multi-component system and experimentally accessible measurable structure factors $S_M(Q)$. While $\langle S(Q) \rangle$ contains only the structural information of self-organizing systems, $S_M(Q)$ is additionally influenced by the optical properties of their constituents, resulting in features such as changing amplitudes, additional peaks in the low-wavevector region or splitting of higher-order maxima, which are not related to structural reasons. It is shown that these effects can be systematically categorized according to the qualitative behaviour of the form factor in the Guinier region, which enables assessing the suitability of experimentally obtained structure factors to genuinely represent the micro-structure of complex systems free from any particular model assumption. Hence, a careful data analysis regarding size distribution and optical properties of single scatterers is mandatory to avoid a misinterpretation of measurable structure factors.

1. Introduction

Colloidal dispersions attract wide interest in condensed matter physics as highly tunable model systems, mimicking atoms and molecules on the much larger mesoscopic scale with typical length scales between 10 and 1000 nm. Studying these systems enabled major advances in the comprehension of the characteristics of simple fluids and solids, which stimulated the progress of significant theoretical developments towards the understanding of complex systems and materials (Lu & Weitz, 2013).

Scattering experiments serve as essential methods for structural and dynamical investigations in colloidal many-particle systems (Li et al., 2016). Small-angle scattering (SANS with neutrons or SAXS with X-rays as a probe) enables the characterization of colloidal suspensions across the entire range of relevant scattering vector magnitudes Q (Glatter, 2018). By employing visible light, which is also a natural choice since its wavelength is of the same order of magnitude as the typical size of a colloidal particle, the same type of analysis is in principle also possible in a simpler laboratory setup. This is however connected with the cost of a limited resolution and, as a consequence thereof, the restriction to comparatively large structures (Bohren & Huffmann, 2008).

In non-interacting systems, the positions and orientations of the colloidal particles are completely uncorrelated. Thus, the scattered intensity results solely from the superposition of the
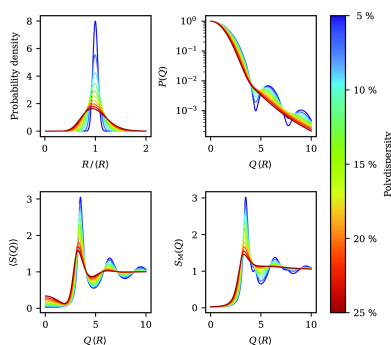
scattering functions of the single constituents. However, when the particles do interact, higher-level structures emerge from inherent self-organization due to interparticle forces, such as electrostatic and steric interactions or van der Waals attractions. The intensity is then influenced both by the optical properties of the scatterers themselves and by the spatial correlations between them. For idealized radially symmetric and monodisperse systems, where all particles are assumed to be identical, the two contributions can be rigorously separated into the form factor $P(Q)$, containing the single-particle properties, and the structure factor $S(Q)$, which encodes the structural correlations, employing the well known factorization $I(Q) \propto P(Q) S(Q)$ (Hansen et al., 1991).

Realistic dispersions typically exhibit a distribution of characteristics, prominently through particle size. In polydisperse interacting systems, the characterization via scattering experiments is in general significantly more complicated, as the factorization of the intensity into form factor and structure factor can no longer be employed in a straightforward way (Salgi & Rajagopalan, 1993). Additionally, the observed diffraction patterns become increasingly featureless for broader size distributions, further obstructing the interpretation of experimental intensities. The analysis of multi-component systems thus requires a thorough understanding of the underlying distributions of scattering properties and particle interactions. Insights can be gained through contrast-variation techniques (Ballauff, 2001); selectively altering the contrast between specific particle types or between particles and the surrounding medium allows for the isolation and probing of distinct species, aiding the validation of theoretical models.

From an experimental standpoint, it is useful to analyse the measurable structure factor $S_M(Q)$, which is defined in such a way that the factorization property $I(Q) \propto P(Q) S_M(Q)$ is also recovered in the polydisperse case (Hansen et al., 1991). $S_M(Q)$ is comparatively easy to access experimentally from the ratio between the intensities of an interacting suspension and a highly diluted non-interacting one. It is as such also widely used as a measure for structural correlations in polydisperse systems, where the height of the principal peak is especially well established as an order parameter (Banchio et al., 1998). Under specific circumstances, this type of analysis can however turn into a serious pitfall: $S_M(Q)$ is also fundamentally affected by optical properties of the particles and not only by their interactions (Salgi & Rajagopalan, 1993).

For certain types of dispersions, some simplifying assumptions can be employed. In dilute suspensions of strongly interacting charged particles, for example, the interparticle distances typically are about an order of magnitude larger than the particle sizes because of the large electrostatic repulsion (Hayter & Penfold, 1981). In such a case, the correlation between the particle positions and the scattering amplitudes can be neglected. This neglect of correlations leads to the 'decoupling approximation', under which $S_M(Q)$ can be decomposed into a structure factor that genuinely represents the averaged structural correlations and weighting factors solely dependent on the scattering amplitudes (Pusey et al.,

1982; Kotlarchyk & Chen, 1983). This type of analysis was also recently used in a SANS study of moderately concentrated poly(N-isopropylacrylamide) microgels (Zhou et al., 2023), where again the importance of an accurate treatment of polydispersity was stressed. Non-spherical particles cause effects in scattering patterns that appear quite similar to those introduced by size dispersity in systems of spherical particles (Pusey et al., 1982). These effects can to a certain degree also be treated within the decoupling approximation (Kotlarchyk & Chen, 1983), whose range of validity has been extensively characterized (Greene et al., 2016). In highly concentrated suspensions, where particles are in close contact, the accuracy of the decoupling approximation is strongly diminished, as in these systems the correlation lengths of the particles' centres of mass are comparable to the correlation lengths inside the particles themselves (Pedersen, 1997). At such high particle volume fractions, excluded volume effects are the predominant contribution to the total interaction potential.

The fundamental interactions in dense colloidal dispersions consisting of spherical particles can to a good approximation be theoretically described with the hard-sphere model (Kirkwood & Boggs, 1942; Widom, 1967). The radial distribution functions of an n-component mixture of hard spheres can be calculated within the Percus–Yevick closure of the Ornstein–Zernike equation (Percus & Yevick, 1958) using Baxter's technique (Baxter, 1970), giving access to the corresponding partial structure factors (Vrij, 1978, 1979; Blum & Stell, 1979, 1980). Building on Vrij's work (Vrij, 1979; van Beurten & Vrij, 1981), Griffith et al. (1987) presented an analytical scattering function of a polydisperse hard-sphere fluid with a Schulz–Flory distribution (Flory, 1936; Schulz, 1939) of particle diameters. Despite their helpfulness, these expressions are not widely used because of their perceived complexity. Nayeri et al. (2009) later extended this approach to core–shell structured hard spheres and used their expressions to describe experimental intensities of a hard-sphere-like microemulsion system. Only recently, Botet et al. (2020) provided expressions for $S_M(Q)$ in a simple accessible form and for a number of commonly encountered size distributions. Their analytical expressions are valid for hard optically homogeneous spheres.

This resurgence of interest is an incentive to systematically examine how different form-factor models affect the characteristics of measurable structure factors. It is a well known fact that, especially in dense dispersions, $S_M(Q)$ is generally not equal to the structure factor $\langle S(Q) \rangle$ representing the averaged spatial correlations of the entire system (Salgi & Rajagopalan, 1993; Frenkel et al., 1986). The mismatch between $S_M(Q)$ and $\langle S(Q) \rangle$ is precisely the reason why in many past studies an extraction of $S_M(Q)$ is deliberately not attempted. By describing the scattered intensity of concentrated suspensions with sophisticated models, a thorough characterization of particle properties is possible without calculating $S_M(Q)$, as performed, for example, by Stieger, Pedersen et al. (2004); Stieger, Richtering et al. (2004); Zackrisson et al. (2005); Balogh et al. (2007); or Scotti (2021).

Certainly, however, for many applications in condensed matter science, gaining an accurate approximation of the

structure factor is still highly desired. This is especially the case when employing computer simulations or many-body theory to model structural phenomena and wanting to compare detailed facets of particle self-organization directly with experimental outcomes (Dekker *et al.*, 2020; Peláez-Fernández *et al.*, 2011; Anta & Madden, 1999; Krause *et al.*, 1991; Stellbrink *et al.*, 2002). Beyond using structure factors to deduct structural patterns from experimental scattering data (Mohanty *et al.*, 2017; Phalakornkul *et al.*, 1996; Scheffold & Mason, 2009; Mason *et al.*, 2006), these quantities are used in theoretical approaches to calculate short- and long-time dynamics in many-particle systems. Two notable examples in this context are the $\delta\gamma$-expansion by Beenakker & Mazur (1983, 1984) used to model hydrodynamic effects during short-time diffusion (Genz & Klein, 1991) and the widely known mode-coupling theory of the glass transition (Janssen, 2018), which both need the static structure factor as an input for calculations. In these theories, a popular method is to circumvent computationally expensive multi-component calculations by considering an effective one-component analysis using the experimentally obtained structure factor $S_M(Q)$ directly, assuming this quantity to be an accurate representation of the average structure factor $\langle S(Q) \rangle$ (Robert *et al.*, 2008; Di Cola *et al.*, 2009).

For a number of specialized cases, deviations between $\langle S(Q) \rangle$ and $S_M(Q)$ and the general influence of varying optical properties on $S_M(Q)$ have already been assessed (Banchio *et al.*, 1998; Pedersen, 2001). The purpose of this contribution is to raise further awareness on how particles' optical properties influence the shape of $S_M(Q)$ while the underlying interactions remain unchanged and to show that these observations can be model-independently systematized on the basis of quite universal principles. This enables practitioners to make informed judgements under which circumstances such an experimentally obtained structure factor can still serve as a valid order parameter. We show typical examples of shapes that can be realistically encountered during contrast-variation experiments, so even without explicitly employing established theoretical models [see *e.g.* Pedersen (1997) for a large collection of scattering functions], a qualitative assessment of experimental findings is possible. We also analyse two simplified models for optically inhomogeneous particles: those with a linear gradient of the scattering contrast and spheres with a core–shell structure. Nevertheless, the approach is readily adaptable to any model and provides a toolbox for the modelling of measurable structure factors for hard-sphere suspensions with arbitrary form factors, as demonstrated in several past studies (Vrij, 1979; Frenkel *et al.*, 1986; Pedersen, 2001; Nayeri *et al.*, 2009; Botet *et al.*, 2020; Diaz Maier & Wagner, 2024).

2. Scattering of hard-sphere mixtures

We consider a mixture of spherical particles, where each particle can be categorized into one of n species. The composition of the mixture is specified by the number fractions $x_\alpha = N_\alpha/N$, where N is the total number of particles and

N_α is the number of particles belonging to species α. We further restrict ourselves to elastic single scattering events where the Born approximation is applicable. In such a case, the mean intensity

$$I(Q) \propto \sum_{\alpha,\beta} (x_\alpha x_\beta)^{1/2} f_\alpha(Q) f_\beta(Q) S_{\alpha\beta}(Q) \tag{1}$$

is proportional to the weighted sum of the single-particle scattering amplitudes $f_\alpha(Q)$ and the partial structure factors $S_{\alpha\beta}(Q)$ (Salgi & Rajagopalan, 1993). Herein, the scattering amplitude

$$f_\alpha(Q) = 4\pi \int_0^\infty \rho_\alpha(r) r^2 \frac{\sin(Qr)}{Qr} \, \mathrm{d}r \tag{2}$$

is the Fourier–Bessel transform of the scattering contrast $\rho_\alpha(r)$, whereas the partial structure factors $S_{\alpha\beta}(Q)$ are obtained from the solution of the multi-component Ornstein–Zernike equation. Expressions for $S_{\alpha\beta}(Q)$ of the hard-sphere fluid within the Percus–Yevick closure are given by Vrij (1979) but, for the convenience of the reader, the solution is re-articulated in Appendix *A*, and presented in a manner that is accessible and easily applicable. This genuine multi-component approach involving partial structure factors is a general and versatile formalism, from which both the decoupling approximation (Kotlarchyk & Chen, 1983) and the local monodisperse approximation (Pedersen, 1994), serving as a localized effective one-component approach suited for very polydisperse systems, can be derived.

For non-interacting particles, the partial structure factors are simply $S_{\alpha\beta}(Q) = \delta_{\alpha\beta}$, where $\delta_{\alpha\beta}$ denotes the Kronecker symbol. Equation (1) then reduces to the size average of the squared scattering amplitudes,

$$I(Q) \propto \langle f^2(Q) \rangle = \sum_\alpha x_\alpha f_\alpha^2(Q). \tag{3}$$

The average form factor

$$P(Q) = \frac{\langle f^2(Q) \rangle}{\langle f^2(0) \rangle} \tag{4}$$

is familiarly obtained from the normalization to forward scattering. As the measurable structure factor should satisfy the relation $I(Q) \propto P(Q) S_M(Q)$, the expression

$$S_M(Q) = \left[\langle f^2(Q) \rangle \right]^{-1} \sum_{\alpha,\beta} (x_\alpha x_\beta)^{1/2} f_\alpha(Q) f_\beta(Q) S_{\alpha\beta}(Q) \tag{5}$$

results from the combination of equations (1) and (3). The averaged structure factor

$$\langle S(Q) \rangle = \sum_{\alpha,\beta} (x_\alpha x_\beta)^{1/2} S_{\alpha\beta}(Q) \tag{6}$$

provides information about the total spatial correlations between all present particles, regardless of their species labels. It represents a true thermodynamic average independent of any optical properties. Any deviation between $S_M(Q)$ and $\langle S(Q) \rangle$ is thus a measure for the perturbation of $\langle S(Q) \rangle$ caused by the scattering amplitudes.

We now want to explore the influence of the scattering amplitudes on the shape of $S_M(Q)$. The aim is to gain a qualitative understanding of generic patterns; so to keep the analysis tractable, only a single representative size distribution is considered. For this purpose, the Schulz–Flory distribution with probability density

$$c(R) = \frac{1}{\Gamma(Z+1)} \left(\frac{Z+1}{\langle R \rangle}\right)^{Z+1} R^Z \exp\left(-\frac{Z+1}{\langle R \rangle}R\right) \quad (7)$$

is chosen. Here, R is the particle radius with mean $\langle R \rangle$ and $\Gamma(x)$ represents the gamma function. The polydispersity p of the system is specified by the shape parameter Z via $p^2 = (\langle R^2 \rangle - \langle R \rangle^2)/\langle R \rangle^2 = 1/(Z + 1)$. The idea is now to discretize the distribution to a representative n-component mixture. For the Schulz–Flory distribution, an efficient way to achieve this is by exploiting the generalized Gauss–Laguerre quadrature rule, specifically used to calculate integrals with a weighting function like equation (7) (D'Aguanno & Klein, 1992; D'Aguanno, 1993; Olver et al., 2010). The nodes and weights generated by such a procedure are equivalent to the particle radii and number fractions of a discrete mixture which shares the first $2n - 1$ moments $\langle R^n \rangle$ with the original continuous distribution. For each calculated scattering function, we carefully checked that the number of nodes necessary for convergence was reached. The numerical scheme was further tested against the analytical $S_M(Q)$ for homogeneous spheres provided by Botet et al. (2020), where excellent agreement was found.

3. Measurable structure factors of polydisperse systems

3.1. General remarks

Fig. 1 provides a general introductory overview of the influence of polydispersity on $P(Q)$, $S_M(Q)$ and $\langle S(Q) \rangle$, discussed for a dense suspension of homogeneous spheres, serving as a reiteration of well known phenomenology (Botet et al., 2020). Concerning the form factors, only those corresponding to polydispersities of less than 10% appear structured. Familiarly, the characteristic minima in $P(Q)$ become increasingly smeared out for broader size distributions.

Polydispersity also causes a change in the initial slope of $P(Q)$ in the Guinier region. Reflecting the distribution of particle sizes when calculating the Taylor expansion of $P(Q)$, the slope is now given by $-Q^2\langle R_G^2 \rangle/3$, where the familiar radius of gyration R_G is substituted by an apparent radius of gyration $\langle R_G^2 \rangle^{1/2}$ (Glatter, 2018; Tomchuk et al., 2014). For homogeneous spheres,

$$\langle R_G^2 \rangle = \frac{3}{5}\frac{\langle R^8 \rangle}{\langle R^6 \rangle} \quad (8)$$
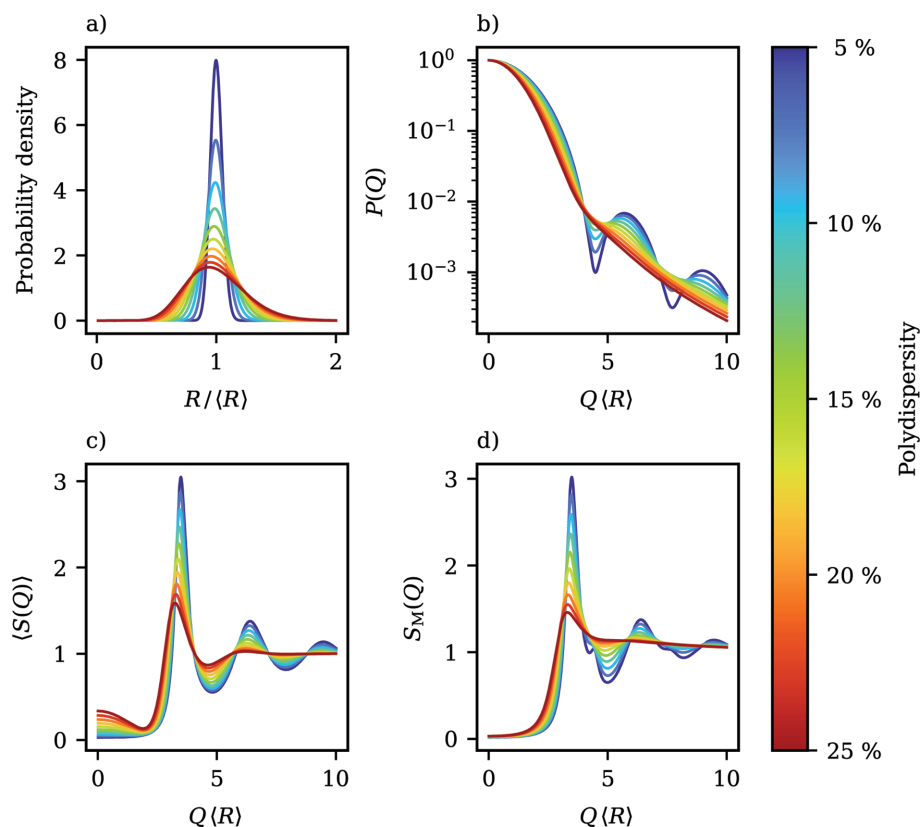

Figure 1
Comparative analysis of scattering functions for an ensemble of optically homogeneous hard spheres with varying degrees of polydispersity. (a) Probability density function illustrating the Schulz–Flory distributed radius R. (b) Form factor $P(Q)$. (c) Average structure factor $\langle S(Q) \rangle$. (d) Measurable structure factor $S_M(Q)$. All evaluated at a total volume fraction of $\varphi = 0.5$, spanning polydispersities from 5 to 25%. $\langle R \rangle$ denotes the mean radius of the spheres.

is obtained, which reduces to the well known result of $R_{\mathrm{G}}^2 = (3/5)R^2$ for monodisperse systems.

Similarly to $P(Q)$, both the measurable structure factor $S_{\mathrm{M}}(Q)$ and the average structure factor $\langle S(Q)\rangle$ become increasingly featureless at high polydispersities, which is distinctively noticeable as the principal peak's amplitude decreases and the secondary oscillations gradually disappear. Shifting the focus to direct comparison between the two structure factors $S_{\mathrm{M}}(Q)$ and $\langle S(Q)\rangle$, multiple observations are apparent. While the amplitude of the principal peak is similar for both functions, differences appear at larger wavevectors, where secondary peaks in $S_{\mathrm{M}}(Q)$ appear at roughly the locations of the form-factor minima, as similarly noticed by Ginoza & Yasutomi (1999). With increasing polydispersity, these maxima evolve into broad shoulders that get smeared out eventually. As also noted by Ginoza & Yasutomi (1999), sharp secondary maxima are hard to observe experimentally because a very narrow size distribution in combination with a homogenous distribution of the scattering length density (SLD) inside the particles is required. On the other hand, shoulder-like features in experimentally determined structure factors are well documented [see, as an example, Di Cola *et al.* (2009)]. In the low-Q region, a striking observation is the significant increase of $\langle S(0)\rangle$ at elevated polydispersities in comparison with $S_{\mathrm{M}}(0)$. According to the fluctuation-dissipation theorem from statistical mechanics, the isothermal compressibility κ_{T} is for monodisperse systems connected to the zero-wavevector limit of $S(Q)$ via $S(0) = \rho k_{\mathrm{B}} T \kappa_{\mathrm{T}}$, where ρ denotes the number density and $k_{\mathrm{B}} T$ is the thermal energy. The extension of this concept to mixtures must however be treated with caution because, for multi-component systems, the connection between structure and thermodynamics is not simply given by the size average $\langle S(0)\rangle$. According to the Kirkwood–Buff theory of solutions, it is instead given by the relation $(\rho k_{\mathrm{B}} T \kappa_{\mathrm{T}})^{-1} = \sum x_\alpha x_\beta S_{\alpha\beta}^{-1}(0)$, where $S_{\alpha\beta}^{-1}(Q)$ is the $\alpha\beta$ element of the inverse structure-factor matrix (Hansen & McDonald, 2013).

3.2. Linear contrast gradient

As a prototypical example for particles with inhomogeneous scattering strength, particles with a linear gradient of the SLD are investigated. This is particularly relevant for swellable particles into which the suspension medium can diffuse. This can occur with microgel particles (Karg *et al.*, 2019), for example. Under certain reaction conditions, an inhomogeneous degree of cross-linking arises, which also leads to inhomogeneous scattering properties. Particles with intrinsic material gradients are also plausible, obtained for example by continuously changing the monomer composition in a feed process during synthesis. Then, in principle, a suspension in which the contrast within a particle changes its sign can also be realized. The form of a linear gradient is assumed for the sake of simplicity in order to investigate the phenomenology of continuous contrasts as an example.

The scattering contrast as a function of the distance r from the centre can for a single particle be parametrized as

$$\rho(r) = \begin{cases} \rho_0 + (\rho_R - \rho_0)\dfrac{r}{R} & \text{if } 0 \le r \le R, \\ 0 & \text{otherwise,} \end{cases} \quad (9)$$

where R is the particle radius, ρ_0 is the contrast in the centre and ρ_R is the contrast at the interface to the surrounding medium. Accordingly, the resulting single-particle scattering amplitude is given by

$$f(Q) = 4\pi \left\{ \rho_0 \frac{\sin(QR) - QR\cos(QR)}{Q^3} + \frac{\rho_R - \rho_0}{R} \right. $$
$$\left. \times \frac{2QR\sin(QR) - [(QR)^2 - 2]\cos(QR) - 2}{Q^4} \right\}, \quad (10)$$

which reduces to

$$f(0) = \pi R^3 \left(\frac{\rho_0}{3} + \rho_R \right) \quad (11)$$

in the forward-scattering limit. A closer look at equation (11) reveals that the forward-scattering contribution disappears if the condition $\rho_R/\rho_0 = -1/3$ is fulfilled. In particular, when the maximum accessible scattering vector is limited, as in the case of light scattering, forward scattering contributes significantly to the total scattering cross section. If the forward scattering is zero, the sample appears almost optically transparent. Refractive-index matching can be achieved for particles with a homogeneous scattering capacity if the SLD of the suspension medium is adapted to that of the particles. If the scattering capacity is inhomogeneous, index matching can only minimize the total scattering cross section, which is often achieved by making the forward scattering almost zero. In the following, the condition when the forward scattering power is minimal is referred to as the index match point.

To gain a systematic understanding of the behaviour of the measurable structure factor $S_{\mathrm{M}}(Q)$ as a function of the contrast ratio ρ_R/ρ_0, it will prove advantageous to investigate the Guinier region of the form factor. Using the contrast profile from equation (9), for a single particle with radius R,

$$R_{\mathrm{G}}^2 = \frac{2}{5} \frac{\rho_0 + 5\rho_R}{\rho_0 + 3\rho_R} R^2 \quad (12)$$

is obtained for the effective squared radius of gyration, which depends not only on the particle's radius but also on the two contrast parameters ρ_0 and ρ_R. For polydisperse suspensions, a similar expression emerges:

$$\langle R_{\mathrm{G}}^2 \rangle = \frac{2}{5} \frac{\rho_0 + 5\rho_R}{\rho_0 + 3\rho_R} \frac{\langle R^8 \rangle}{\langle R^6 \rangle}. \quad (13)$$

As such, the contrast dependence of the prefactor is not altered by polydispersity and the qualitative discussion can instead be based on monodisperse suspensions. We will thus refer to the prefactor simply as R_{G}^2/R^2, even in the polydisperse case.

Inspecting equation (12), several characteristic ratios ρ_R/ρ_0 are apparent: R_{G}^2 becomes zero for $\rho_R/\rho_0 = -1/5$; exhibits a pole at $\rho_R/\rho_0 = -1/3$, incident with the index match point; and has an asymptotic limit of $R_{\mathrm{G}}^2/R^2 = 2/3$ for $\rho_R/\rho_0 \to \pm\infty$. Here, it will be shown that the behaviour of the scattering

functions can be divided into three qualitatively distinct classes, and that form factors and measurable structure factors within each domain share unique features. The classification based on the behaviour of R_G^2, together with form factors $P(Q)$ and measurable structure factors $S_M(Q)$ representative of each region, is visualized in Fig. 2. The regions are characterized as follows:

(I) For $\rho_R/\rho_0 > -1/5$, R_G^2 is positive and the form factors have the familiar decaying shape known from homogeneous spheres. With decreasing contrast ratio, the decay becomes increasingly gradual until $R_G^2 = 0$ is reached for $\rho_R/\rho_0 = -1/5$. Around the principal peak of $S_M(Q)$ and for lower wavevectors, changes in the contrast have a negligible influence on the measurable structure factors. However, at wavevectors beyond the principal peak's location, $S_M(Q)$ is greatly affected by contrast variation. Depending on the specific location of the first form-factor minimum, which shifts to larger wavevectors with lower contrast ratios, the shoulder-like artefact also visible in Fig. 1 moves through $S_M(Q)$ towards larger wavevectors and therein most prominently affects the shape of the first local minimum and the following secondary maximum.

(II) For the contrast ratios $-1/3 < \rho_R/\rho_0 < -1/5$, R_G^2 becomes negative, which implies an imaginary radius of gyration R_G leading to a positive initial slope of $P(Q)$. Form factors in this region therefore initially increase from $P(0) = 1$ until a global maximum is reached at $QR \simeq 4$, after which they decay. The height of the maximum increases as the contrast ratio moves towards the index match point at $\rho_R/\rho_0 = -1/3$. Curiously, the measurable structure factors in this domain are almost indistinguishable, even though the variation of R_G^2 is much more pronounced in comparison with region (I), where the span of R_G^2 is small but $S_M(Q)$ shows a much more diverse behaviour. Also, the distorting artefacts from region (I) disappear almost completely.

(III) Contrast ratios of $\rho_R/\rho_0 < -1/3$ again result in positive R_G^2 and negative initial slopes. Close to the index match point, where R_G^2 is comparatively large, $P(Q)$ exhibits an intriguing shape. At small wavevectors, a pronounced minimum occurs even in very polydisperse suspensions. Beyond the minimum, $P(Q)$ rises to a global maximum reminiscent of region (II). For contrasts in this range, an additional local maximum in $S_M(Q)$ appears at low wavevectors, caused by the presence of the first form-factor minimum. Such secondary maxima are often
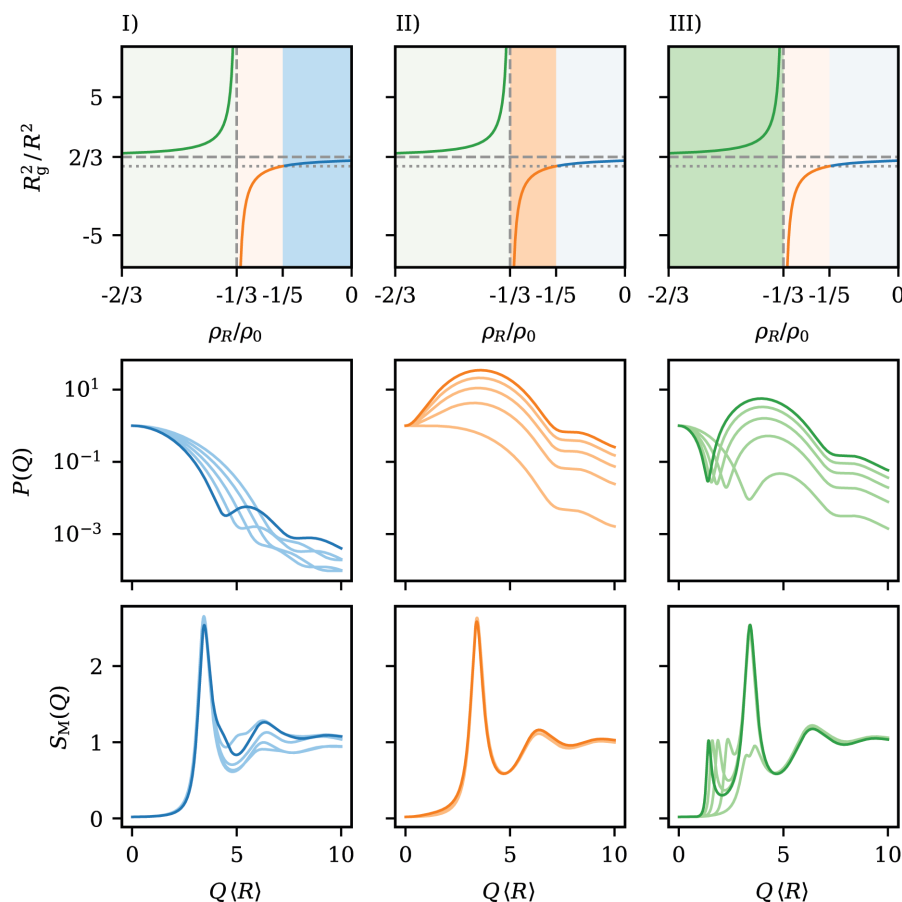

Figure 2
An illustrative breakdown of the classification of the scattering functions of spheres with a linear contrast gradient into the three regimes discussed in the main text, where each column corresponds to a unique region. In the top row, the reduced squared radius of gyration R_G^2/R^2 as a function of the contrast ratio ρ_R/ρ_0 is depicted. The location of the respective regions labelled (I), (II) or (III) is indicated by the darker shaded area. The middle and bottom rows display selected form factors $P(Q)$ and measurable structure factors $S_M(Q)$ that exemplify each region's variability in the shape observed during contrast variation. $\langle R \rangle$ indicates the mean radius of the particles. Note the shared axes of $P(Q)$ and $S_M(Q)$ between rows and columns.

discussed in the literature as an indication of self-organization on length scales beyond the distance of nearest neighbours, *i.e.* the formation of correlated clusters (Sciortino *et al.*, 2004; Liu *et al.*, 2005). The secondary maxima occurring here are exclusively caused by the scattering amplitudes and cannot be attributed to structural properties of the sample. This constitutes a valuable example of a situation where a careless inspection of experimentally determined $S_M(Q)$ can in the worst case lead to unjustified assumptions about the structure of a system. Moving further away from the index match point, the first form-factor minimum moves towards larger wavevectors and gets shallower. At the same time, the following maximum declines and, as such, the shape of $P(Q)$ morphs back into the familiar decaying shape from region (I). Simultaneously, the location of the secondary maximum in $S_M(Q)$ drifts towards higher wavevectors. Fig. 2 also displays a situation where the form-factor minimum exactly coincides with the location where the principal peak of $S_M(Q)$ would normally occur. In this case, the main peak is drastically diminished, which is again not an indicator for a less pronounced short-range order in this particular instance, but can certainly be mistaken as such.

The principal-peak height of a structure factor is an often employed structural order parameter. Scheffold & Mason (2009) noticed in their investigation of highly concentrated nanoemulsions that the peak amplitude in $S_M(Q)$ is deeply affected by polydispersity. As such, the evolution of this height during contrast variation is also of special interest. Fig. 3 compares the peak height of the average structure factor $\langle S(Q_{max})\rangle$ with the value of $S_M(Q_{max})$ at the same wavevector as a function of the contrast ratio ρ_R/ρ_0 and for different degrees of polydispersity. Overall, it is clearly shown that $S_M(Q_{max})$ is deeply affected by changes in the contrast. There exist two contrast ratios where $S_M(Q_{max})$ and $\langle S(Q_{max})\rangle$ coincide. One of them is to a good approximation given by $\rho_R/\rho_0 \simeq -1/5$, the location where the apparent radius of gyration disappears and $P(Q)$ decays very slowly. The other location is at a positive contrast ratio and drifts towards higher

ρ_R/ρ_0 with increasing polydispersity. Bounded by those two ratios is a regime where $S_M(Q_{max})$ exceeds $\langle S(Q_{max})\rangle$, while for all other contrast ratios, the peak height from $S_M(Q_{max})$ underestimates the actual height. For comparatively small polydispersities around 5%, the deviation from $\langle S(Q_{max})\rangle$ is small and only amounts to a few per cent, as long as the contrast ratio is larger than $\rho_R/\rho_0 \simeq -1/5$. For lower ratios, $S_M(Q_{max})$ is strongly diminished, most pronouncedly at contrast ratios of $\rho_R/\rho_0 \simeq -1$. For higher polydispersities, the deviations become even more severe, as best visualized in Fig. 3(*b*), where the relative deviation between $\langle S(Q_{max})\rangle$ and $S_M(Q_{max})$ is depicted. Even in the immediate vicinity of $\langle S(Q_{max})\rangle = S_M(Q_{max})$, already deviations of the order of 5–10% appear for the highest shown polydispersities. This demonstrates that, no matter what the actual degree of polydispersity, $S_M(Q_{max})$ can only serve as a reliable order parameter for very specific contrast ratios.

3.3. Core–shell particles

Core–shell models are commonly employed to describe particles consisting of different layers of material, *e.g.* nanoparticles with grafted stabilizer shells (Hallett *et al.*, 2020; Diaz Maier & Wagner, 2024) or micellar structures (Szymusiak *et al.*, 2017). As core and shell naturally differ in their material properties, in principle both positive and negative contrast differences with respect to the surrounding medium can occur, similarly to particles with continuous material gradients. For Schulz–Flory-distributed core–shell particles, analytical expressions for the form factor $P(Q)$ exist in the case of a polydisperse core and a shell of constant thickness (Bartlett & Ottewill, 1992), for a polydisperse total diameter and a constant core-to-shell ratio (Wagner, 2004), and for both core radius and shell thickness independently distributed (Wagner, 2012). Moreover, an analytical solution for the problem of correlated hard-sphere core–shell systems was provided by Nayeri *et al.* (2009).

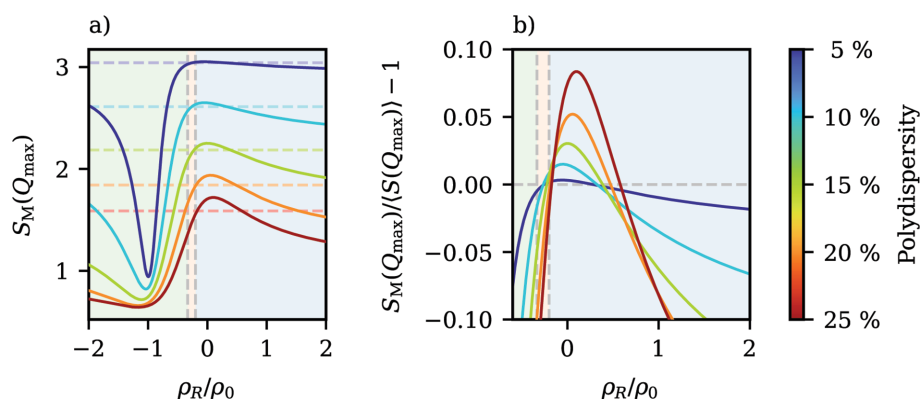The scattering amplitude of a single core–shell particle,

Figure 3
(*a*) The influence of the contrast ratio ρ_R/ρ_0 on the principal-peak value $S_M(Q_{max})$ for spheres with a linear contrast gradient, for polydispersities in a range between 5 and 25% at a total volume fraction of $\varphi = 0.5$. The horizontal dashed lines mark, for comparison, the height of the principal peak of the average structure factor $\langle S(Q_{max})\rangle$. The distinction between the different introduced contrast regimes from Fig. 2 is indicated by the vertical dashed lines. (*b*) Relative deviation between $S_M(Q_{max})$ and $\langle S(Q_{max})\rangle$ for an enlarged region.

$$f(Q) = 4\pi \left[(\rho_c - \rho_s) \frac{\sin(QR_c) - QR_c \cos(QR_c)}{Q^3} + \rho_s \frac{\sin(QR) - QR \cos(QR)}{Q^3} \right], \quad (14)$$

is the sum of the amplitudes of a sphere and a spherical shell, weighted by their respective contrasts, ρ_c and ρ_s. R_c and R are the core radius and the total radius of the particle, respectively, and we specifically consider the case where the core radius and the total radius are connected by a constant species-independent size ratio $\delta = R_c/R$.

Similar to the gradient model, the forward-scattering contribution

$$f(0) = \frac{4}{3}\pi R^3 \left[\delta^3 (\rho_c - \rho_s) + \rho_s \right] \quad (15)$$

disappears for specific contrast combinations of the ratio of contrasts $\rho_s/\rho_c = \delta^3/(\delta^3 - 1)$, which now additionally depends on the size ratio δ. For the effective radius of gyration of a polydisperse system, an expression with similar structure to equation (13) emerges:

$$\langle R_G^2 \rangle = \frac{3}{5} \frac{\delta^5 \rho_c + (1 - \delta^5)\rho_s}{\delta^3 \rho_c + (1 - \delta^3)\rho_s} \frac{\langle R^8 \rangle}{\langle R^6 \rangle}. \quad (16)$$

That, again, a prefactor containing the contrasts can be decoupled from the size average is a peculiarity of this model with constant size ratio and a key reason why this assumption was made for this investigation.

In Fig. 4, the contrast dependence of R_G^2/R^2 is visualized for different size ratios δ. As in the case of spheres with a linear gradient of the SLD, this results in hyperbola-like curves,
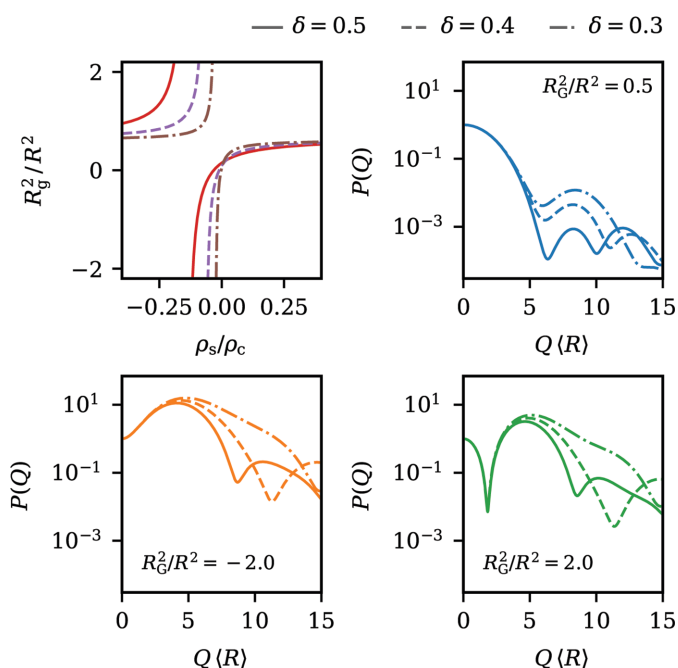
where the location of the pole is now influenced by δ; an increasing ratio of core diameter to total diameter shifts the location of the pole to more negative contrast ratios (ρ_s/ρ_c). The contrast ratio where $R_G^2 = 0$ is, in comparison, only slightly altered by δ. This leads to a larger range of contrast ratios with negative R_G^2 as the shell thickness decreases.

This shows that core–shell particles exhibit qualitatively comparable optical characteristics to particles with a linear density gradient. As such, the form factors $P(Q)$ of core–shell systems can likewise be categorized into three classes based on their behaviour at low wavevectors. Example form factors for each class are also visualized in Fig. 4.

Because of these similarities, we focus the remainder of the discussion on aspects that are unique to core–shell particles, i.e. how measurable structure factors are influenced by
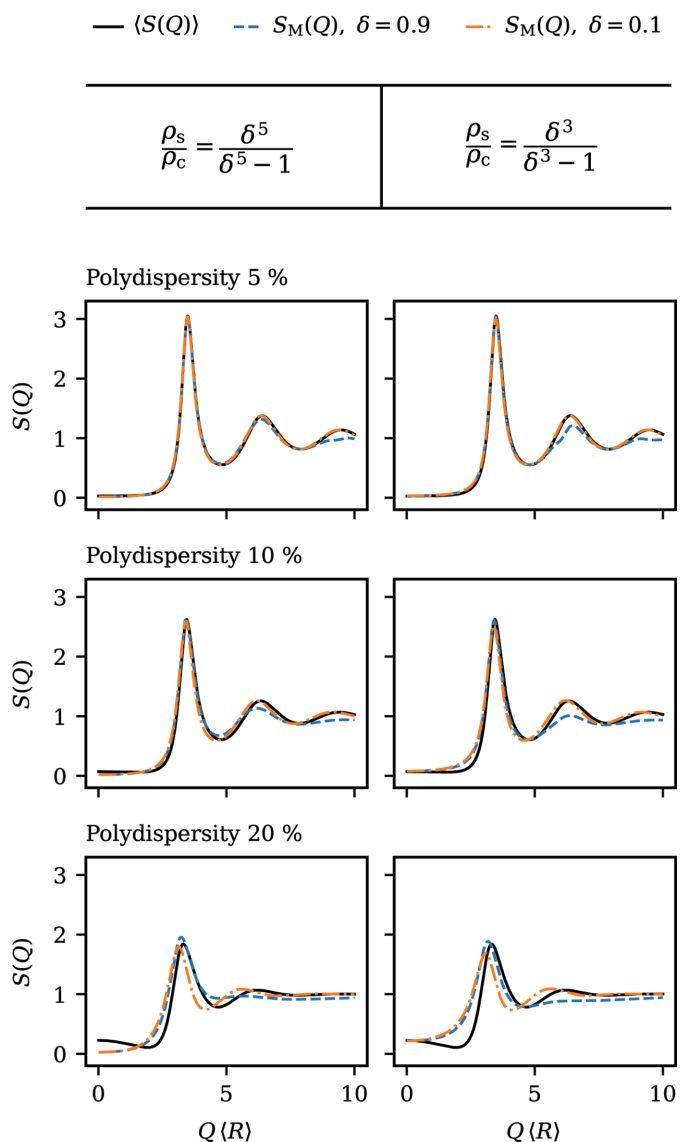

Figure 4
The influence of the contrast ratio ρ_s/ρ_c on the reduced squared radius of gyration R_G^2/R^2 for core–shell particles with different ratios δ between core radius and total radius, along with three representative sets of form factors, each sharing the same radius of gyration for different size ratios.

Figure 5
Comparison between measurable structure factor $S_M(Q)$ and size-averaged structure factor $\langle S(Q) \rangle$ of core–shell particles for different core-to-total ratios (δ), contrast ratios (ρ_s/ρ_c) and polydispersities as indicated in the figure. The total volume fraction for all shown structure factors is $\varphi = 0.5$.

different core-to-shell ratios. For this purpose, structure factors corresponding to two important edge cases, particles with a small core and particles with a thin shell, are compared in Fig. 5 for different degrees of polydispersity and chosen contrast ratios ρ_s/ρ_c. Core–shell models with thin shells are often encountered when characterizing particles stabilized by a grafted polymer layer, which are prototypical colloidal model particles displaying hard-sphere behaviour (Royall *et al.*, 2013). The case of hard spheres with a strongly scattering small core and a weakly scattering comparatively large shell is equally of interest. Under these conditions, essentially, the behaviour of highly charged strongly repelling particles whose interparticle distance is several times larger than their diameter is artificially mimicked. For these systems, the measurable structure factor $S_M(Q)$ should in theory to a good approximation coincide with the average structure factor $\langle S(Q) \rangle$. To reasonably compare models with different size ratios (δ), two specific contrast ratios (ρ_s/ρ_c) are depicted: the ratio $\rho_s/\rho_c = \delta^3/(\delta^3 - 1)$ at the index matching point, where forward scattering is minimized; and the ratio $\rho_s/\rho_c = \delta^5/(\delta^5 - 1)$, where $\langle R_G^2 \rangle = 0$ and $P(Q)$ shows the weakest decay. In the case of $\delta \ll 1$, both conditions basically lead to the same result: the shell is virtually hidden with $\rho_s \simeq 0$.

As can be observed in Fig. 5, for moderate polydispersities of 5–10%, the small core-to-total ratio $\delta = 0.1$ indeed yields measurable structure factors $S_M(Q)$ that are indistinguishable from $\langle S(Q) \rangle$ for both depicted contrast ratios. For particles with thin shells ($\delta = 0.9$), $S_M(Q)$ and $\langle S(Q) \rangle$ also agree well in the vicinity of the principal peak. However, differences arise around the secondary maxima, where the peak amplitudes in $S_M(Q)$ are diminished because of the interference of the scattering amplitudes. With increasing polydispersity, this deviation becomes more pronounced. Still, even for particles that are seemingly quite close to homogeneous spheres, artefacts in $S_M(Q)$ can be significantly reduced by careful contrast variation.

Looking at highly polydisperse systems, it is evident that, even for rather small cores with $\delta = 0.1$, $\langle S(Q) \rangle$ cannot be accurately represented by any $S_M(Q)$. Only the height of the principle peak is correctly estimated. This stresses again the importance of an accurate treatment of very broad size distributions, where any kind of approximation must be carefully checked for validity.

4. Conclusions

Colloidal dispersions generally exhibit a particle size distribution, which needs to be taken into account when interpreting results from scattering experiments. The measurable structure factor $S_M(Q)$ is an experimental, comparatively easily accessible measure for the interparticle structure in interacting systems. However, in polydisperse systems, $S_M(Q)$ is, beyond the structural correlations, also decisively affected by the optical properties of the individual particles. To this end, we systematically investigated the influence of different form-factor models on the shape of $S_M(Q)$ of dense dispersions with hard-sphere interactions. The characterization of

measurable structure factors was extended to two classes of spherical particles with inhomogeneous scattering capacity: first, spheres with a linear SLD profile as a general model for particles with continuous contrast gradients and, second, a core–shell system as a prototype for particles with layered structures.

For both models, we find that the structure factors can be categorized into three distinctive classes of shared qualitative features, based on the behaviour of the form factor $P(Q)$ in the Guinier region. $S_M(Q)$ can, for these optically inhomogeneous model particles, be significantly influenced by the variation of the scattering contrasts relative to the surrounding medium. Depending on the specific contrast combination, shoulder-like features emerge, maxima are diminished or split, and even secondary maxima in the low-wavevector region, reminiscent of cluster peaks, can be observed. These effects are solely due to the optical properties of the particles and are not caused by structural changes in the sample. We further showed that the height of the principal peak of $S_M(Q)$ can only be regarded as a representative order parameter in a very restricted range of contrasts, especially for broad size distributions.

These observations emphasize the need to properly address the distribution of particle size (and possibly also other characteristics) in the interpretation of static scattering experiments. Actually, for many applications, deliberately broad size distributions are a desired feature; an academically relevant example is studies of deeply supercooled glass-forming systems (Ninarello *et al.*, 2017), where crystallization needs to be suppressed and where polydispersity effects in any form certainly cannot be neglected (Zaccarelli *et al.*, 2015; Pihlajamaa *et al.*, 2023).

Beyond providing an enhanced qualitative understanding of features that can possibly be encountered when analysing experimentally extracted measurable structure factors, the numerical scheme presented in this contribution in principle provides a means to model the scattered intensity of any polydisperse hard-sphere system, provided a model for the single-particle scattering amplitude and an appropriate size distribution is available. Performing fits with such advanced models directly on experimentally observed intensities gives access to the underlying partial structure factors, enabling a characterization and possible further theoretical analysis on a genuine multi-component foundation, rather than employing effective one-component approaches. The current restriction to hard-sphere interactions is a major incentive to promote advancements in the analytical evaluation of partial structure factors for other interaction potentials, since numerically solving integral equations or employing computer simulations with reasonable statistics are currently only realistically feasible for a restricted number of components, especially in mixtures with large size disparities (Allahyarov *et al.*, 2022).

APPENDIX A
Percus–Yevick structure factors for hard-sphere mixtures

The analytical solution of the Ornstein–Zernike equation for the hard-sphere potential within the Percus–Yevick closure in

terms of the partial structure factors $S_{\alpha\beta}(Q)$, presented by Vrij (1979) and reformulated by Voigtmann (2003), is restated here. In short, an expression for the partial direct correlation functions $c_{\alpha\beta}(r)$ in real space can be found using Baxter's factorization technique (Baxter, 1970). The transformed solution in wavevector space $c_{\alpha\beta}(Q)$ can subsequently be used to obtain the partial structure factors $S_{\alpha\beta}(Q)$.

Let φ be the total volume fraction of all spheres, d_α be the diameter and x_α be the number fraction of the spheres of species α. The total number density ρ of the system is related to the volume fraction by $\varphi = (\pi/6)\rho \sum x_\alpha d_\alpha^3$. With the abbreviations

$$d_{\alpha\beta} = \frac{d_\alpha + d_\beta}{2} \tag{17}$$

and

$$\xi_x = \frac{\pi}{6}\rho \sum_\gamma x_\gamma d_\gamma^x, \tag{18}$$

the set of coefficients

$$a_\alpha = \frac{1 - \xi_3 + 3d_\alpha\xi_2}{(1 - \xi_3)^2}, \tag{19}$$

$$\tilde{a}_2 = \sum_\gamma \rho_\gamma a_\gamma^2, \tag{20}$$

$$\hat{\beta}_0 = \frac{9\xi_2^2 + 3\xi_1(1 - \xi_3)}{(1 - \xi_3)^3}, \tag{21}$$

$$A_{\alpha\beta} = \frac{d_{\alpha\beta}(1 - \xi_3) + \frac{3}{2}d_\alpha d_\beta\xi_2}{(1 - \xi_3)^2}, \tag{22}$$

$$B_{\alpha\beta} = \frac{1}{1 - \xi_3} - \hat{\beta}_0 d_\alpha d_\beta \tag{23}$$

and

$$D_{\alpha\beta} = \frac{6\xi_2 + 12d_{\alpha\beta}[\xi_1 + 3\xi_2^2/(1 - \xi_3)]}{(1 - \xi_3)^2} \tag{24}$$

can be determined. Furthermore, by introducing $S_\alpha = \sin(Qd_\alpha/2)$ and $C_\alpha = \cos(Qd_\alpha/2)$, the terms

$$\mu_A = A_{\alpha\beta}\frac{S_\alpha S_\beta - C_\alpha C_\beta}{Q^2}, \tag{25}$$

$$\mu_B = B_{\alpha\beta}\frac{C_\alpha S_\beta + C_\beta S_\alpha}{Q^3}, \tag{26}$$

$$\mu_D = D_{\alpha\beta}\frac{S_\alpha S_\beta}{Q^4} \tag{27}$$

and

$$\tilde{\mu} = \frac{4\pi}{Q^4}\tilde{a}_2\left(\frac{C_\alpha C_\beta d_\alpha d_\beta}{4} + \frac{S_\alpha S_\beta}{Q^2} - \frac{C_\alpha S_\beta d_\alpha + C_\beta S_\alpha d_\beta}{2Q}\right) \tag{28}$$

can be calculated, which finally leads to

$$c_{\alpha\beta}(q) = -4\pi\left(\mu_A + \mu_B + \mu_D + \tilde{\mu}\right). \tag{29}$$

The partial direct correlation functions form the matrix $\mathbf{C}$ with elements $C_{\alpha\beta} = (x_\alpha x_\beta)^{1/2}c_{\alpha\beta}$, which is related to the matrix of partial structure factors $\mathbf{S}$ by the Ornstein–Zernike relation

$$\mathbf{S} = [\mathbf{1} - \rho\,\mathbf{C}]^{-1}. \tag{30}$$

The partial structure factors here are defined within the convention $\lim_{Q\to\infty} S_{\alpha\beta}(Q) = \delta_{\alpha\beta}$, where $\delta_{\alpha\beta}$ is the Kronecker delta.

References

Allahyarov, E., Löwen, H. & Denton, A. R. (2022). *Phys. Chem. Chem. Phys.* **24**, 15439–15451.
Anta, J. A. & Madden, P. A. (1999). *J. Phys. Condens. Matter*, **11**, 6099–6111.
Ballauff, M. (2001). *Curr. Opin. Colloid Interface Sci.* **6**, 132–139.
Balogh, J., Olsson, U. & Pedersen, J. S. (2007). *J. Phys. Chem. B*, **111**, 682–689.
Banchio, A. J., Nägele, G. & Ferrante, A. (1998). *J. Colloid Interface Sci.* **208**, 487–499.
Bartlett, P. & Ottewill, R. H. (1992). *J. Chem. Phys.* **96**, 3306–3318.
Baxter, R. J. (1970). *J. Chem. Phys.* **52**, 4559–4562.
Beenakker, C. W. J. & Mazur, P. (1983). *Physica A*, **120**, 388–410.
Beenakker, C. W. J. & Mazur, P. (1984). *Physica A*, **126**, 349–370.
Beurten, P. van & Vrij, A. (1981). *J. Chem. Phys.* **74**, 2744–2748.
Blum, L. & Stell, G. (1979). *J. Chem. Phys.* **71**, 42–46.
Blum, L. & Stell, G. (1980). *J. Chem. Phys.* **72**, 2212.
Bohren, C. F. & Huffman, D. R. (2008). *Absorption and Scattering of Light by Small Particles.* New York: John Wiley.
Botet, R., Kwok, S. & Cabane, B. (2020). *J. Appl. Cryst.* **53**, 1570–1582.
D'Aguanno, B. (1993). *Phys. Scr.* **T49A**, 84–88.
D'Aguanno, B. & Klein, R. (1992). *Phys. Rev. A*, **46**, 7652–7656.
Dekker, F., Kuipers, B. W. M., González García, Á., Tuinier, R. & Philipse, A. P. (2020). *J. Colloid Interface Sci.* **571**, 267–274.
Diaz Maier, J. & Wagner, J. (2024). *Soft Matter*, **20**, 1309–1319.
Di Cola, E., Moussaïd, A., Sztucki, M., Narayanan, T. & Zaccarelli, E. (2009). *J. Chem. Phys.* **131**, 144903.
Flory, P. J. (1936). *J. Am. Chem. Soc.* **58**, 1877–1885.
Frenkel, D., Vos, R. J., de Kruif, C. G. & Vrij, A. (1986). *J. Chem. Phys.* **84**, 4625–4630.
Genz, U. & Klein, R. (1991). *Physica A*, **171**, 26–42.
Ginoza, M. & Yasutomi, M. (1999). *J. Phys. Soc. Jpn*, **68**, 2292–2297.
Glatter, O. (2018). *Scattering Methods and their Application in Colloid and Interface Science.* Amsterdam: Elsevier.
Greene, D. G., Ferraro, D. V., Lenhoff, A. M. & Wagner, N. J. (2016). *J. Appl. Cryst.* **49**, 1734–1739.
Griffith, W. L., Triolo, R. & Compere, A. L. (1987). *Phys. Rev. A*, **35**, 2200–2206.
Hallett, J. E., Grillo, I. & Smith, G. N. (2020). *Langmuir*, **36**, 2071–2081.
Hansen, J.-P., Levesque, D. & Zinn-Justin, J. (1991). *Liquids, Freezing and Glass Transition.* Amsterdam: North Holland.
Hansen, J.-P. & McDonald, I. R. (2013). *Theory of Simple Liquids with Applications to Soft Matter.* Amsterdam: Elsevier.
Hayter, J. B. & Penfold, J. (1981). *Mol. Phys.* **42**, 109–118.
Janssen, L. M. C. (2018). *Front. Phys.* **6**, 97.
Karg, M., Pich, A., Hellweg, T., Hoare, T., Lyon, L. A., Crassous, J. J., Suzuki, D., Gumerov, R. A., Schneider, S., Potemkin, I. I. & Richtering, W. (2019). *Langmuir*, **35**, 6231–6255.

Kirkwood, J. G. & Boggs, E. M. (1942). *J. Chem. Phys.* **10**, 394–402.

Kotlarchyk, M. & Chen, S.-H. (1983). *J. Chem. Phys.* **79**, 2461–2469.

Krause, R., D'Aguanno, B., Mendez-Alcaraz, J. M., Nägele, G., Klein, R. & Weber, R. (1991). *J. Phys. Condens. Matter*, **3**, 4459–4475.

Li, T., Senesi, A. J. & Lee, B. (2016). *Chem. Rev.* **116**, 11128–11180.

Liu, Y., Chen, W.-R. & Chen, S.-H. (2005). *J. Chem. Phys.* **122**, 044507.

Lu, P. J. & Weitz, D. A. (2013). *Annu. Rev. Condens. Matter Phys.* **4**, 217–233.

Mason, T. G., Graves, S. M., Wilking, J. N. & Lin, M. Y. (2006). *J. Phys. Chem. B*, **110**, 22097–22102.

Mohanty, P. S., Nöjd, S., van Gruijthuijsen, K., Crassous, J. J., Obiols-Rabasa, M., Schweins, R., Stradner, A. & Schurtenberger, P. (2017). *Sci. Rep.* **7**, 1487.

Nayeri, M., Zackrisson, M. & Bergenholtz, J. (2009). *J. Phys. Chem. B*, **113**, 8296–8302.

Ninarello, A., Berthier, L. & Coslovich, D. (2017). *Phys. Rev. X*, **7**, 021039.

Olver, F. W. J., Lozier, D. W., Boisvert, R. F. & Clark, C. W. (2010). *The NIST Handbook of Mathematical Functions*. Cambridge University Press.

Pedersen, J. S. (1994). *J. Appl. Cryst.* **27**, 595–608.

Pedersen, J. S. (1997). *Adv. Colloid Interface Sci.* **70**, 171–210.

Pedersen, J. S. (2001). *J. Chem. Phys.* **114**, 2839–2846.

Peláez-Fernández, M., Moncho-Jordá, A. & Callejas-Fernández, J. (2011). *J. Chem. Phys.* **134**, 054905.

Percus, J. K. & Yevick, G. J. (1958). *Phys. Rev.* **110**, 1–13.

Phalakornkul, J. K., Gast, A. P., Pecora, R., Nägele, G., Ferrante, A., Mandl-Steininger, B. & Klein, R. (1996). *Phys. Rev. E*, **54**, 661–675.

Pihlajamaa, I., Laudicina, C. C. L. & Janssen, L. M. C. (2023). *Phys. Rev. Res.* **5**, 033120.

Pusey, P. N., Fijnaut, H. M. & Vrij, A. (1982). *J. Chem. Phys.* **77**, 4270–4281.

Robert, A., Wagner, J., Härtl, W., Autenrieth, T. & Grübel, G. (2008). *Eur. Phys. J. E*, **25**, 77–81.

Royall, C. P., Poon, W. C. K. & Weeks, E. R. (2013). *Soft Matter*, **9**, 17–27.

Salgi, P. & Rajagopalan, R. (1993). *Adv. Colloid Interface Sci.* **43**, 169–288.

Scheffold, F. & Mason, T. G. (2009). *J. Phys. Condens. Matter*, **21**, 332102.

Schulz, G. V. (1939). *Z. Phys. Chem.* **43B**, 25–46.

Sciortino, F., Mossa, S., Zaccarelli, E. & Tartaglia, P. (2004). *Phys. Rev. Lett.* **93**, 055701.

Scotti, A. (2021). *Soft Matter*, **17**, 5548–5559.

Stellbrink, J., Allgaier, J., Richter, D., Moussaid, A., Schofield, A. B., Poon, W. C. K., Pusey, P. N., Lindner, P., Dzubiella, J., Likos, C. N. & Löwen, H. (2002). *Appl. Phys. Mater. Sci. Process.* **74**, s355–s357.

Stieger, M., Pedersen, J. S., Lindner, P. & Richtering, W. (2004). *Langmuir*, **20**, 7283–7292.

Stieger, M., Richtering, W., Pedersen, J. S. & Lindner, P. (2004). *J. Chem. Phys.* **120**, 6197–6206.

Szymusiak, M., Kalkowski, J., Luo, H., Donovan, A. J., Zhang, P., Liu, C., Shang, W., Irving, T., Herrera-Alonso, M. & Liu, Y. (2017). *ACS Macro Lett.*, **6**, 1005–1012.

Tomchuk, O. V., Bulavin, L. A., Aksenov, V. L., Garamus, V. M., Ivankov, O. I., Vul', A. Y., Dideikin, A. T. & Avdeev, M. V. (2014). *J. Appl. Cryst.* **47**, 642–653.

Voigtmann, T. (2003). *Mode Coupling Theory of the Glass Transition in Binary Mixtures*, Technische Universität München.

Vrij, A. (1978). *J. Chem. Phys.* **69**, 1742–1747.

Vrij, A. (1979). *J. Chem. Phys.* **71**, 3267–3270.

Wagner, J. (2004). *J. Appl. Cryst.* **37**, 750–756.

Wagner, J. (2012). *J. Appl. Cryst.* **45**, 513–516.

Widom, B. (1967). *Science*, **157**, 375–382.

Zaccarelli, E., Liddle, S. M. & Poon, W. C. K. (2015). *Soft Matter*, **11**, 324–330.

Zackrisson, M., Stradner, A., Schurtenberger, P. & Bergenholtz, J. (2005). *Langmuir*, **21**, 10835–10845.

Zhou, B., Gasser, U. & Fernandez-Nieves, A. (2023). *Phys. Rev. E*, **108**, 054604.